

NLO Higgs boson production via vector-boson fusion matched with shower in POWHEG

Paolo Nason

INFN, Sezione di Milano-Bicocca, Piazza della Scienza 3, 20126 Milan, Italy
E-mail: Paolo.Nason@mib.infn.it

Carlo Oleari

Università di Milano-Bicocca and INFN, Sezione di Milano-Bicocca
Piazza della Scienza 3, 20126 Milan, Italy
E-mail: Carlo.Oleari@mib.infn.it

ABSTRACT: We present a next-to-leading order calculation of Higgs boson production in vector-boson fusion processes interfaced to shower Monte Carlo programs, implemented according to the POWHEG method.

KEYWORDS: QCD, Monte Carlo, NLO Computations, Resummation, Collider Physics .

Contents

1. Introduction	1
2. The POWHEG implementation	2
2.1 The POWHEG BOX	2
2.2 Tagging parton lines	4
2.3 Tuning the real cross section in POWHEG	6
2.4 The CKM-matrix treatment	6
3. Results	7
4. Conclusions	14

1. Introduction

Higgs boson production via vector-boson fusion (VBF) is expected to provide a copious source of Higgs bosons in pp -collisions at the Large Hadron Collider (LHC) at CERN. It can be visualized (see fig. 1(a)) as the inelastic scattering of two quarks (antiquarks), mediated by t -channel W or Z exchange, with the Higgs boson radiated off the weak bosons. It represents (after gluon fusion) the second most important production process for Higgs boson studies [1, 2]. Once the Higgs boson has been found and its mass determined, the measurement of its couplings to gauge bosons and fermions will be of main interest [3, 4]. Here VBF will play a central role since it will be observed in the $H \rightarrow \tau\tau$ [5, 6], $H \rightarrow WW$ [7, 8] and $H \rightarrow \gamma\gamma$ [9] channels. This multitude of channels allows to probe the different Higgs boson couplings. The VBF measurements can be performed at the LHC with statistical accuracies of the order of 5 to 10% [3]. In addition, in order to distinguish the VBF Higgs boson signal from backgrounds, stringent cuts are required on the Higgs boson decay products as well as on the two forward quark jets which are characteristic for VBF. The efficiency of these cuts has to be evaluated on the basis of the most updated simulation tools and experimental inputs. It is typically of the order of 25%.

In the past few years, the next-to-leading order (NLO) corrections to Higgs boson production in VBF have become available [10, 11, 12] and implemented in fully-flexible partonic Monte Carlo programs (see, for example, the VBFNLO package [13] and the MCFM code [14]). The NLO QCD corrections have been shown to be modest [10], of order 5 to 10% in most cases, but reaching 30% in some distributions. In addition, scale uncertainties range from 5% or less for distributions to below $\pm 2\%$ for the Higgs boson total cross section after typical VBF cuts.

In addition, the dominant NLO corrections to $Hjjj$ in VBF have been computed in ref. [15]. In refs. [16, 17, 18, 19], interference of VBF and Higgsstrahlung, electroweak corrections and loop-induced interference effects have been computed too, and it was shown that, in the phase-space region relevant for VBF observation at the LHC, these effects are small, so that they can be neglected at first approximation.

In this work we merge the NLO calculation of Higgs boson production via VBF with a shower Monte Carlo program, according to the POWHEG method. This method was first suggested in ref. [20], and was described in great detail in ref. [21]. Until now, the POWHEG method has been applied to ZZ pair hadroproduction [22], heavy-flavour production [23], e^+e^- annihilation into hadrons [24] and into top pairs [25], Drell-Yan vector boson production [26, 27], W' production [28], Higgs boson production via gluon fusion [29, 30], Higgs boson production associated with a vector boson (Higgs-strahlung) [30], single-top production [31] and $Z + 1$ jet production [32]. Unlike the MC@NLO implementation [33], POWHEG produces events with positive (constant) weight, and, furthermore, does not depend on the subsequent shower Monte Carlo program. It can be easily interfaced to any modern shower generator and, in fact, it has been interfaced to HERWIG [34, 35] and PYTHIA [36] in refs. [22, 23, 26, 29, 31].

This paper is organized as follows. In section 2 we briefly introduce the POWHEG BOX package, that will be discussed in great detail in a forthcoming paper [37]. We describe some of its new features (that were not present in previous POWHEG implementations) needed in order to deal with Higgs production in VBF in a more efficient way. In section 3 we show our results for several typical kinematic variables, often discussed when dealing with VBF Higgs boson production.

Since this is the first NLO plus shower implementation of Higgs boson production in VBF, we could not make any comparison with other similar results. We limit ourselves to make comparisons among the pure NLO distributions and the POWHEG results showered by HERWIG 6.510 and PYTHIA 6.4.21. Finally, in section 4, we give our conclusions.

2. The POWHEG implementation

2.1 The POWHEG BOX

We have implemented VBF Higgs boson production inside the POWHEG BOX [37]. This is an automated package that turns a NLO calculation into a POWHEG one, and whose output are events ready to be showered by any shower Monte Carlo program, such as HERWIG or PYTHIA. All the details and an explanation of how it works will be given in a forthcoming paper [37].

In order to build a POWHEG implementation using the POWHEG BOX, one has to provide the following:

- a) A list of all flavour structures of the Born processes.
- b) The Born squared amplitude \mathcal{B} and the Born phase space.

- c) The color correlated \mathcal{B}_{ij} and spin correlated $\mathcal{B}_{\mu\nu}$ Born cross sections. These are common ingredients in NLO calculations regularized with a subtraction method.
- d) The Born color structure in the large limit of the number of colors.
- e) The finite part of the virtual corrections \mathcal{V}_{fin} , computed in dimensional regularization or in dimensional reduction.
- f) The list of all the flavour structures of the real processes.
- g) The real matrix elements squared for all relevant partonic processes.

The POWHEG BOX then finds all the singular regions, builds the soft and collinear counterterms and the soft and collinear remnants, and then generates the radiation with the POWHEG Sudakov form factor.

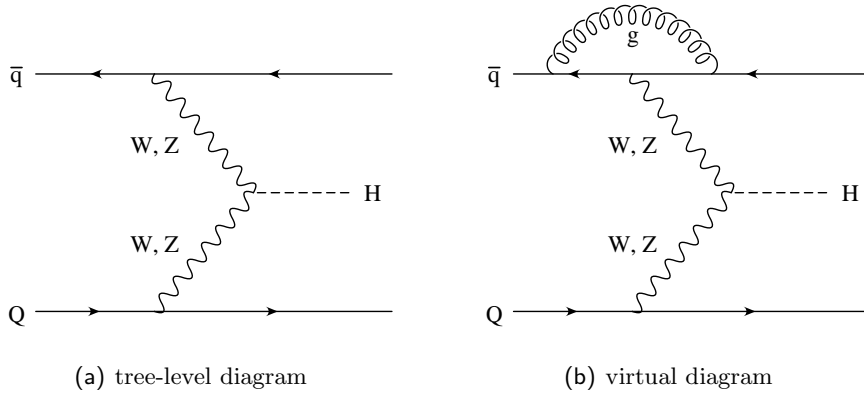


Figure 1: Feynman graphs contributing to $\bar{q}(1) Q(2) \rightarrow H(3) \bar{q}(4) Q(5)$ at tree level (a) and including virtual corrections to the upper quark line (b).

At lowest order, Higgs boson production via vector-boson fusion is represented by a single Feynman graph, like the one depicted in fig. 1(a) for $\bar{q}(1) Q(2) \rightarrow H(3) \bar{q}(4) Q(5)$. The numbers in parenthesis represent a collective index that identifies flavour, color, spin and momentum of the corresponding particle. Strictly speaking, the single Feynman graph picture is valid only for different quark flavours on the two fermion lines. For identical flavours, annihilation processes, like $\bar{q}q \rightarrow Z^* \rightarrow ZH$ with subsequent decay $Z \rightarrow \bar{q}q$, or similar WH production channels, contribute as well. In addition, for $qq \rightarrow Hqq$ or $\bar{q}\bar{q} \rightarrow H\bar{q}\bar{q}$, the interchange of identical quarks in the initial or final state needs to be considered in principle. However, in the phase-space regions where VBF can be observed experimentally, with widely separated quark jets of very large invariant mass, the interference of these additional graphs is strongly suppressed by large momentum transfer in the weak-boson propagators. Furthermore, color suppression makes these effects negligible. In the following we systematically neglect any identical-fermion effects.

At NLO, all the vertex corrections (see an example in fig. 1(b)) and all the real emission diagrams (see fig. 2 for a couple of representative diagrams) must be included. Because of the color singlet nature of the exchanged weak boson, any interference term between

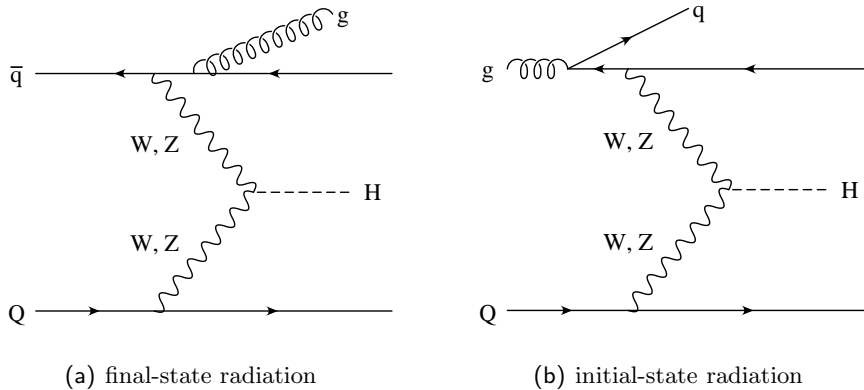


Figure 2: Sample of real-emission contributions to Higgs boson production via vector-boson fusion. Corrections for the upper quark line only are shown: final-state gluon radiation (a) and initial-state radiation process (b).

sub-amplitudes with gluons attached to both the upper and the lower quark lines vanishes identically at order α_s .

We have computed all the amplitudes numerically, using the helicity-amplitude formalism of refs. [38, 39], in a similar way to what was done in ref. [10].

The virtual corrections are particularly simple, since they factorize on the Born squared amplitude \mathcal{B} . Following the notation of eq. (2.92) of ref. [21], the finite part of the virtual corrections, once an appropriate normalization term is factorized in front, is given by

$$\mathcal{V}_{\text{fin}} = C_F \left[-\log^2 \left(-\frac{\mu_R^2}{q_1^2} \right) - 3 \log \left(-\frac{\mu_R^2}{q_1^2} \right) - \log^2 \left(-\frac{\mu_R^2}{q_2^2} \right) - 3 \log \left(-\frac{\mu_R^2}{q_2^2} \right) + 2c_v \right] \mathcal{B}, \quad (2.1)$$

where μ_R is the renormalization scale, q_1 and q_2 are the space-like momenta of the two exchanged weak bosons, and $c_v = -8$ in dimensional regularization. Since there are no external gluons at the Born level, all the spin correlated Born amplitudes $\mathcal{B}_{\mu\nu}$ are zero. From color conservation along the upper or lower line, we can easily derive that the symmetric matrix of color correlated Born cross section \mathcal{B}_{ij} has elements

$$\mathcal{B}_{14} = \mathcal{B}_{25} = C_F \mathcal{B}, \quad (2.2)$$

all other elements being zero.

The Born total cross section is finite. For this reason we could generate events with no cuts at the partonic level at leading order (LO). The Born phase space then covers the entire phase space. Although, in principle, VBF generation cuts could be applied, we had no need to do that since a large number of events can be easily generated.

Since there is only one Feynman diagram at Born level with only quarks, the assignment of color flow is straightforward and unambiguous, and follows directly the propagation of quarks and/or antiquarks.

2.2 Tagging parton lines

In Higgs boson production via VBF, it is convenient to treat the upper quark line as distinct from the lower one (see fig. 1). In fact, radiation from the upper quark line has no interfer-

ence with radiation from the lower line, due to color flow (colorless particle exchanged in the t channel). Since the POWHEG BOX searches for radiation regions automatically, it does not in principle consider the upper and lower VBF lines as distinct. Consider for example the real graph depicted in fig. 3. It corresponds to a gluon-initiated next-to-leading cor-

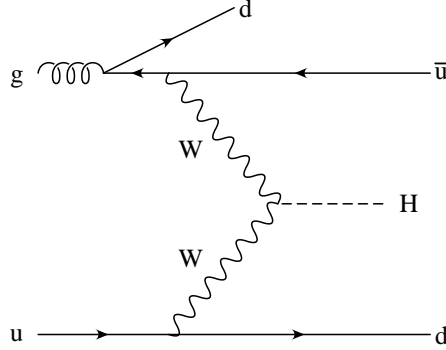


Figure 3: Example of NLO gluon-initiated correction to Higgs boson production in VBF: $gu \rightarrow H\bar{u}dd$.

rection to VBF Higgs boson production: $gu \rightarrow H\bar{u}dd$. It is clear that the two d quarks in the final state have a very different role, and should be kept distinct. However, as far as the flavour combinatorics is concerned, they are considered identical in the POWHEG BOX, that assumes that the graphs are already symmetrized with respect to identical final-state particles. Thus, the combinatoric algorithm will generate two regions for this graph, corresponding to either d being collinear to the incoming gluon. In order to overcome this problem, the POWHEG BOX allows the possibility to attribute a tag to each line, so that lines with the same flavour but different tags will be treated differently from the combinatoric point of view. In the example at hand, one assigns the tags according to the scheme in figure 4. We arbitrarily assign a tag equal to zero to particles that we do not need to tag (the initial-state gluon and the produced Higgs boson). Within this scheme of assigning

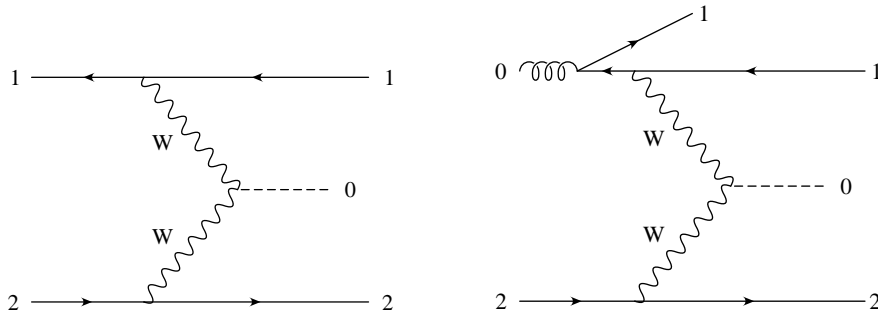


Figure 4: Tag assignment for the underlying Born graph $\bar{d}u \rightarrow H\bar{u}d$ and its gluon-initiated real diagram $gu \rightarrow H\bar{u}dd$.

the tags, the two final-state d quarks will be treated as different from the combinatoric

point of view. Only the quark tagged as 1 in the real graph will generate a singular region, since if quark 2 were collinear to the incoming gluon, the associated underlying Born would have an incoming antiquark tagged as 2, and thus would not be present.

Once the different singular regions have been found, the tag has no further use and the POWHEG BOX proceeds in the generation of radiation in the usual way (see ref. [21, 37]).

2.3 Tuning the real cross section in POWHEG

In POWHEG it is possible to tune the contribution to the real cross section that is treated with the Monte Carlo shower technique. This was pointed out first in ref. [20], where the POWHEG method was formulated, and it was first implemented in ref. [29]. In POWHEG there is the possibility to separate the real cross section, in a given singular region α , as follows

$$R^\alpha = R_s^\alpha + R_f^\alpha, \quad (2.3)$$

where R_f^α has no singularities and only R_s^α is singular in the corresponding region. In practice, the separation may be achieved, for example, using a function of the transverse momentum of the radiation $0 \leq F(k_T^2) \leq 1$, that approaches 1 when its argument vanishes, and define

$$R_s^\alpha = R^\alpha F(k_T^2), \quad (2.4)$$

$$R_f^\alpha = R^\alpha [1 - F(k_T^2)]. \quad (2.5)$$

One carries out the whole POWHEG-style generation using R_s^α rather than R^α . The contribution R_f^α , being finite, is generated with standard NLO techniques, and fed into a shower Monte Carlo as is. This feature is implemented in the POWHEG BOX.

More generally F can be chosen as a general function of the kinematic variables, provided it approaches 1 in the singular region. This turns out to be useful in all cases when the ratio R/B (real over Born cross section) in the POWHEG Sudakov exponent becomes too much larger than its corresponding collinear or soft approximation (see for example ref. [26]). In this case, radiation generation becomes highly inefficient. In Higgs boson production via VBF, we have chosen the function F in the following way: if the real squared amplitude (no parton distribution functions included), in a particular singular region, is greater than five times its soft and collinear approximation, then F is set to zero, otherwise is set to one. This theta-function type choice could be also made milder, but we have found it to work well in this case. We also stress that this procedure remedies automatically to the Born zeros problem examined in ref. [26].

2.4 The CKM-matrix treatment

In the calculation of the partonic matrix elements, all partons have been treated as massless. This gives rise to a different treatment of quark flavours for diagrams where a Z boson or a W boson is exchanged in the t channel. In fact, for all Z -exchange contributions, the b -quark is included as an initial and/or final-state massless parton. The b -quark contributions are quite small, however, affecting the Higgs boson production cross section at the 3% level only. For W -exchange contributions, no initial b -quark has been considered, since it would

have produced mostly a t quark in the final state, that would have been misleadingly treated as massless.

In the POWHEG generation of events, we have used a diagonal form (equal to the identity matrix) for the Cabibbo-Kobayashi-Maskawa (CKM) matrix V_{CKM} . In this way we reduce the number of possible Feynman diagrams (and consequently of singular regions) to a minimal set. At this stage, this approximation is not a limitation of our calculation, as long as no final-state quark flavour is tagged (no c tagging is done, for example). In fact the sum over all flavours, using the exact V_{CKM} , is equivalent to the result obtained using the identity matrix, due to unitarity.

At the end of the generation of radiation done by POWHEG, just before the event is showered by a specific shower Monte Carlo program, the final state quarks are “reweighted” according to the following CKM matrix

$$V_{\text{CKM}} = \begin{array}{c} \\ u \\ c \\ t \end{array} \begin{array}{ccc} d & s & b \\ \left(\begin{array}{ccc} 0.9748 & 0.2225 & 0.0036 \\ 0.2225 & 0.9740 & 0.041 \\ 0.009 & 0.0405 & 0.9992 \end{array} \right), \end{array} \quad (2.6)$$

and the final-state quark flavour is changed accordingly. An example will illustrate this issue more clearly. Let’s suppose that we have generated a POWHEG kinematics for the subprocess $us \rightarrow Hd\bar{c}g$, using an identity matrix for V_{CKM} . We first concentrate on the upper leg, where we have the decay $u \rightarrow W^+d$. We retain the d -quark flavour in the final state with probability equal to V_{ud}^2/Σ , where $\Sigma = V_{ud}^2 + V_{us}^2 + V_{ub}^2$, while we change it to an s -quark or b -quark flavour according to the probabilities V_{us}^2/Σ and V_{ub}^2/Σ , respectively. The lower line undergoes a similar treatment, but for the $s \rightarrow W^-c$ subprocess: the final-state c quark is retained with a probability equal to V_{cs}^2/Σ' , where $\Sigma' = V_{us}^2 + V_{cs}^2 + V_{ts}^2$, while it is changed into a u or a t quark with probability equal to V_{us}^2/Σ' and V_{ts}^2/Σ' , respectively. The case of a t -quark production is, in all cases, disregarded at the end.

3. Results

In this section we present comparisons of the fixed order next-to-leading calculation and the results obtained after the shower performed by HERWIG 6.510 and PYTHIA 6.4.21. We have used the CTEQ6M [40] set for the parton distribution functions and the associated value of $\Lambda_{\overline{\text{MS}}}^{(5)} = 0.226$ GeV. Furthermore, as discussed in refs. [21, 22], we use a rescaled value $\Lambda_{\text{MC}} = 1.569 \Lambda_{\overline{\text{MS}}}^{(5)}$ in the expression for α_s appearing in the Sudakov form factors, in order to achieve next-to-leading logarithmic accuracy.

Although the matrix-element calculation has been performed in the massless-quark limit, the lower cutoff in the generation of the radiation has been fixed according to the mass of the emitting quark. The lower bound on the transverse momentum for the emission off a massless emitter (u, d, s) has been set to the value $p_{\text{T}}^{\text{min}} = \sqrt{5} \Lambda_{\text{MC}}$. We instead choose $p_{\text{T}}^{\text{min}}$ equal to m_c or m_b when the gluon is emitted by a charm or a bottom quark, respectively. We set $m_c = 1.55$ GeV and $m_b = 4.95$ GeV.

The renormalization μ_R and factorization μ_F scales have been taken equal to the transverse momentum of the radiated parton during the generation of radiation, as the POWHEG method requires. The transverse momentum of the radiated parton is taken, in the case of initial-state radiation, as exactly equal to the transverse momentum of the parton with respect to the beam axis. For final-state radiation one takes instead

$$p_T^2 = 2E^2(1 - \cos \theta), \quad (3.1)$$

where E is the energy of the radiated parton and θ the angle it forms with respect to the final-state parton that has emitted it, both taken in the partonic center-of-mass frame.

We have also taken into account properly the heavy-flavour thresholds in the running of α_S and in the parton distribution functions (pdf's), by changing the number of active flavours when the renormalization or factorization scales cross a mass threshold. In the \bar{B} calculation, instead, μ_R and μ_F have been chosen equal to the Higgs boson mass, whose value has been fixed to $m_H = 120$ GeV, and its corresponding width $\Gamma_H = 0.00437$ GeV. The other relevant parameters are

$$M_W = 79.964 \text{ GeV}, \quad M_Z = 91.188 \text{ GeV}, \quad \sin^2 \theta_W^{\text{eff}} = 0.23102, \quad \alpha_{\text{em}}^{-1}(M_Z) = 128.930, \quad (3.2)$$

and we have also set $\Gamma_W = \Gamma_Z = 0$ in all the propagators. From the above values, the weak coupling has been computed as $g = \sqrt{4\pi\alpha_{\text{em}}}/\sin \theta_W^{\text{eff}}$.

Using the POWHEG BOX, we have generated 500000 events that we have interfaced both with HERWIG and with PYTHIA, for an energy of 14 TeV at the LHC pp collider. Events with a top quark in the final state have been neglected, for the reasons discussed in section 2.4.

The defining feature of weak-boson fusion events at hadron colliders is the presence of two forward tagging jets, which, at LO, correspond to the two scattered quarks in the process $\bar{q}Q \rightarrow H\bar{q}Q$. Their observation, in addition to exploiting the properties of the Higgs boson decay products, is crucial for the suppression of backgrounds [5, 6, 7, 8, 9, 41, 42]. The stringent acceptance requirements on the tagging jets imply that their distributions must be known precisely for a reliable prediction of the SM Higgs signal rate. We remind the reader that comparison of the observed Higgs boson production rate with this SM cross section allows to determine its couplings [3, 4]. The theoretical error on the cross section thus directly feeds into the uncertainty of measured couplings.

Since the Higgs boson is a scalar, it does not induce any spin correlation in its decay products. We concentrate then only on the analysis of tagging-jet distributions and we do not impose cuts on the Higgs boson decay products.

After the shower, the final state consists of a Higgs boson plus a number of jets originating from the POWHEG hard partons and from the shower. Jets are defined according to the k_T algorithm [43], as implemented in the FASTJET package [44], setting $R = 0.7$ and imposing the following cuts on their transverse momentum and rapidity

$$p_{Tj} > 20 \text{ GeV}, \quad |y_j| < 5. \quad (3.3)$$

The two tagging jets are the two jets with highest p_T . They must satisfy the additional constraints

$$p_T^{\text{tag}} > 30 \text{ GeV}, \quad |y_{j_1} - y_{j_2}| > 4.2, \quad y_{j_1} \cdot y_{j_2} < 0, \quad m_{jj} > 600 \text{ GeV}, \quad (3.4)$$

i.e. they must be well separated in rapidity, lie in opposite hemispheres and have a large invariant mass.

Only one quarter of the whole number of generated events passes all the cuts, and we have used only these events for the following analysis.

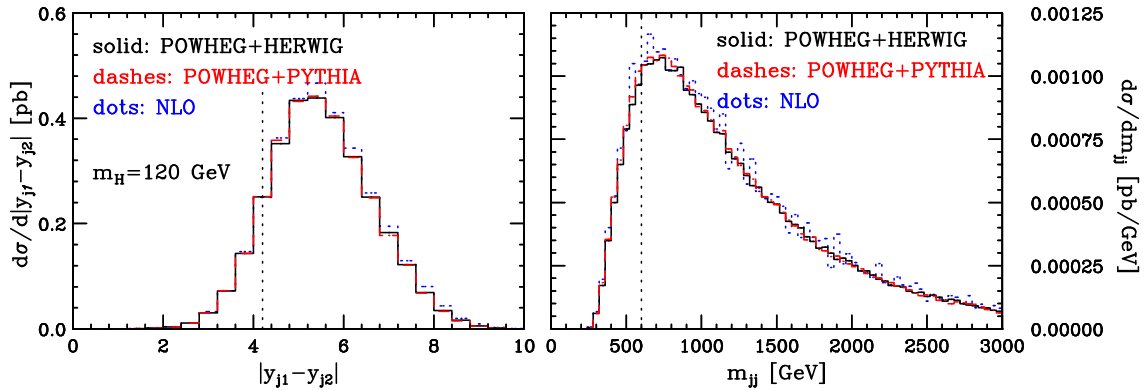


Figure 5: Differential cross section as function of the absolute value of the difference of the rapidity of the two tagging jets (left panel) and of their invariant mass (right panel). In the left panel, we have excluded the $|y_{j_1} - y_{j_2}| > 4.2$ cut of eq. (3.4), while in the right panel we have excluded the $m_{jj} > 600$ GeV constraint. The black dotted line marks the position of these cuts.

In fig. 5 we present the differential cross section as function of the absolute value of the difference of the rapidity of the two tagging jets and of their invariant mass. The characteristic features of the VBF Higgs boson production are left unchanged by the shower: the differential cross section has a peak around 5.5 in the absolute difference of the rapidity of the two tagging jets and the invariant dijet mass still peaks for values around 700 GeV. The NLO curve and the POWHEG results, after the HERWIG and PYTHIA shower, are almost indistinguishable. This result validates the use of the two main cuts (on the difference in rapidity and on the invariant dijet mass) as crucial selection criteria to reduce the background to this process.

In fig. 6 we plot the transverse momentum of the third hardest jet (left panel) and the azimuthal distance between the two tagging jets, $\Delta\phi_{jj}$ (right panel). This last quantity is of particular interest since it is sensitive to the CP nature of the Higgs boson couplings [45, 46, 47, 48]. For example, in gluon-fusion Higgs boson production plus two jets, the analysis of the azimuthal-angle correlations provides for a direct measurement of the CP properties of the $Ht\bar{t}$ Yukawa coupling which is responsible for the effective Hgg vertex. In the VBF process $q(p_1) Q(p_2) \rightarrow H(p_3) q(p_4) Q(p_5)$, the matrix element squared is proportional to

$$|\mathcal{A}_{\text{VBF}}|^2 \propto \frac{1}{(2p_1 \cdot p_4 + M_V^2)^2} \frac{1}{(2p_2 \cdot p_5 + M_V^2)^2} \hat{s} m_{jj}^2, \quad (3.5)$$

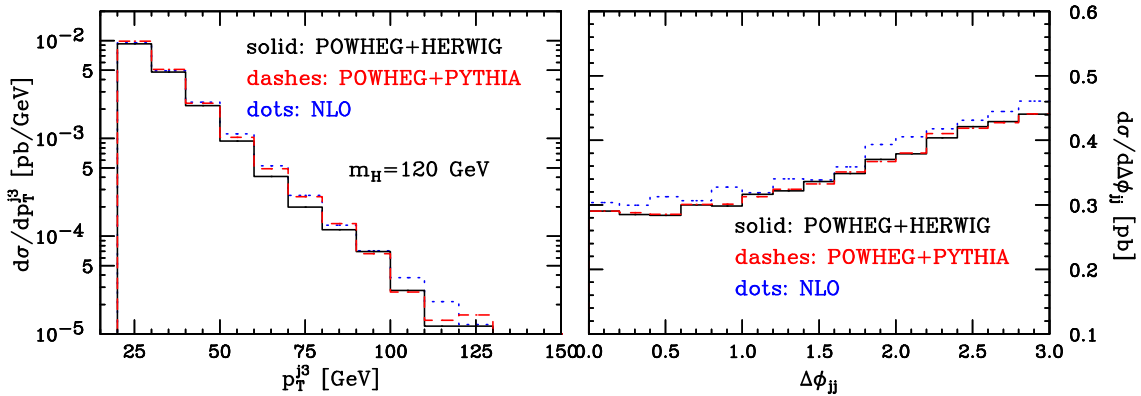


Figure 6: Transverse momentum ($p_T^{j_3}$) distribution of the third hardest jet (left panel) and azimuthal-distance distribution of the two tagging jets, $\Delta\phi_{jj}$ (right panel).

where M_V is the mass of the exchanged t -channel vector boson, and is dominated by the contribution in the forward region, where the dot-products in the denominator are small. Since the dependence of m_{jj}^2 on $\Delta\phi_{jj}$ is mild, we have the flat behavior depicted in fig. 6. Good agreement is found in the two POWHEG results and both agree with the NLO differential cross section.

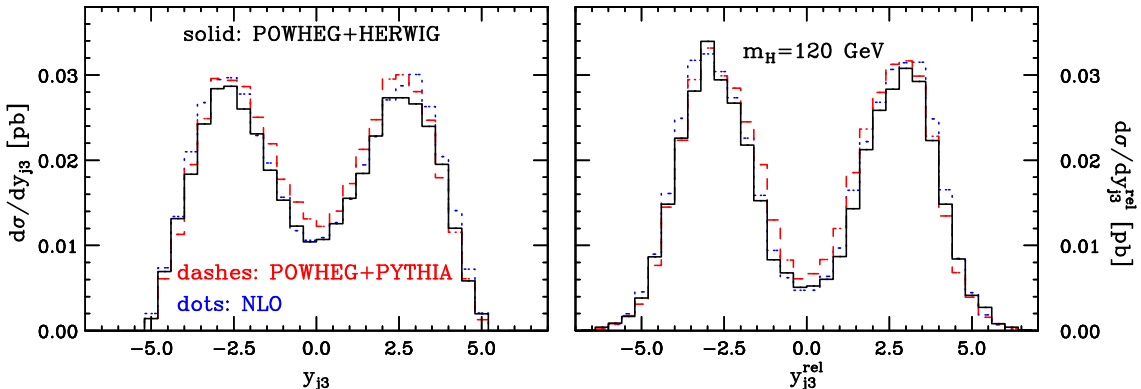


Figure 7: Rapidity y_{j_3} of the third hardest jet (the one with highest p_T after the two tagging jets) on the left panel and rapidity of the same jet with respect to the average of the rapidities of the two tagging jets $y_{j_3}^{\text{rel}} = y_{j_3} - (y_{j_1} + y_{j_2})/2$ on the right panel.

An additional feature characterizing VBF Higgs boson production is the fact that, at leading order, no colored particle is exchanged in the t channel so that no t -channel gluon exchange is possible at NLO, once we neglect, as stated in section 2.1, the small contribution due to equal-flavour quark scattering with $t \leftrightarrow u$ interference. The different gluon radiation pattern expected for Higgs boson production via VBF compared to its major backgrounds ($t\bar{t}$ production, QCD $WW + 2$ jet and QCD $Z + 2$ jet production) is at the core of the central-jet veto proposal, both for light [8] and heavy [49] Higgs boson searches. A veto of any additional jet activity in the central-rapidity region is expected to suppress the backgrounds more than the signal, because the QCD backgrounds are characterized by quark or gluon exchange in the t -channel. The exchanged partons, being

colored, are expected to radiate off more gluons.

For the analysis of the Higgs boson coupling to gauge bosons, Higgs boson + 2 jet production via gluon fusion may also be treated as a background to VBF. When the two jets are separated by a large rapidity interval, the scattering process is dominated by gluon exchange in the t -channel. Therefore, like for the QCD backgrounds, the bremsstrahlung radiation is expected to occur everywhere in rapidity. An analogous difference in the gluon radiation pattern is expected in $Z + 2$ jet production via VBF fusion versus QCD production [50]. In order to analyze this feature, in ref. [51] the distribution in rapidity of the third jet was considered in Higgs + 3 jet production via VBF and via gluon fusion, using cuts similar to the ones in eqs. (3.3) and (3.4). The analysis was done at the parton level only. It showed that, in VBF, the third jet prefers to be emitted close to one of the tagging jets, while, in gluon fusion, it is emitted anywhere in the rapidity region between the tagging jets. Thus, at least with regard to the hard radiation of a third jet, the analysis of refs. [51, 52, 53] confirmed the general expectations about the bremsstrahlung patterns in Higgs production via VBF versus gluon fusion.

To study the distribution of the third hardest jet (the one with highest p_T after the two tagging jets), we plot in fig. 7 its rapidity and its rapidity with respect to the average of the rapidities of the two tagging jets

$$y_{j_3}^{\text{rel}} = y_{j_3} - \frac{y_{j_1} + y_{j_2}}{2}. \quad (3.6)$$

The distributions obtained using POWHEG interfaced to HERWIG and PYTHIA, are very similar and turn out to be well modeled by the respective distributions of the NLO jet: the third jet generally tends to be emitted in the vicinity of either of the tagging jets.

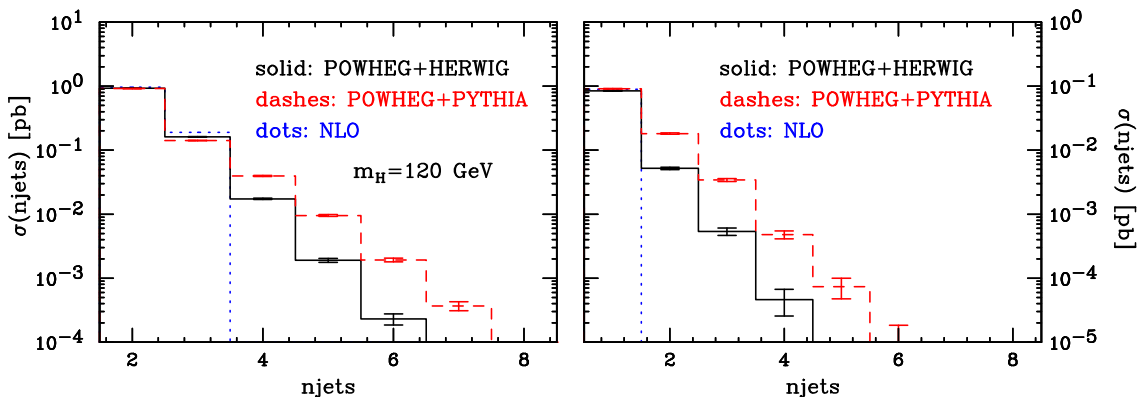


Figure 8: Jet-multiplicity distribution for jets that pass the cuts of eqs. (3.3) and (3.4) (left panel) and those that fall within the rapidity interval of the two tagging jets, $\min(y_{j_1}, y_{j_2}) < y_j < \max(y_{j_1}, y_{j_2})$ (right panel).

In order to quantify the jet activity, we plot the jet-multiplicity distribution for jets that pass the cuts of eqs. (3.3) and (3.4) in the left panel of fig. 8. Again, the first two tagging jets and the third jet are well represented by the NLO cross section, that obviously cannot contribute to events with more than three jets. From the 4th jet on, the showers

of HERWIG and PYTHIA produce sizable differences (note the log scale of the plot), the jets from PYTHIA being harder than those from the HERWIG shower.

A similar behavior is present when we investigate the jet activity restricted in the rapidity interval between the tagging jets. In the right panel of fig. 8 we plot the jet-multiplicity distribution for jets that fall within the rapidity interval of the two tagging jets (also called veto jets), i.e.

$$\min(y_{j_1}, y_{j_2}) < y_j < \max(y_{j_1}, y_{j_2}). \quad (3.7)$$

No difference is seen for the NLO jet with respect to the results of POWHEG interfaced to HERWIG and PYTHIA, while for multiplicity greater than one, PYTHIA generates harder jets if compared to HERWIG.

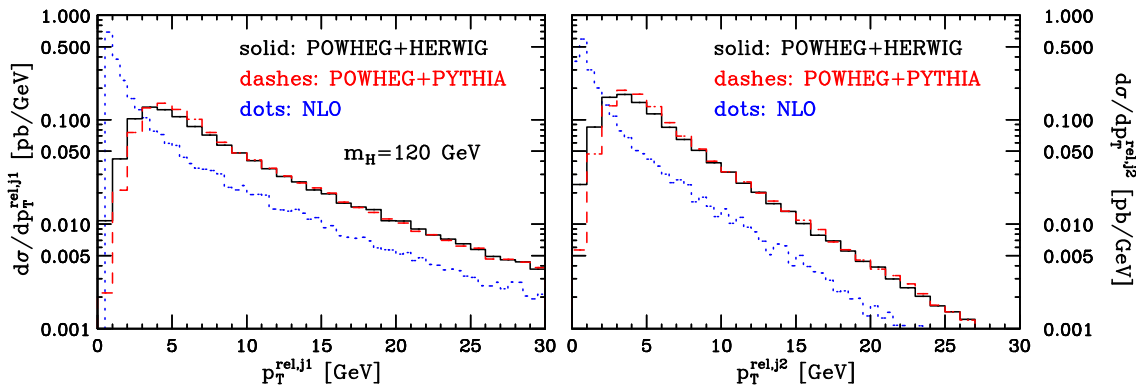


Figure 9: Relative transverse momentum of all the particles clustered inside one of the two tagging jets, in the reference frame where that jet has zero rapidity, defined according to eq. (3.8). In the left panel p_T^{rel,j_1} is plotted while in the right panel we plotted p_T^{rel,j_2} .

Striking differences between the NLO results and POWHEG can be seen, as expected, if we consider distributions sensitive to the collinear/soft regions, such as the relative transverse momentum of all the particles clustered inside one of the two tagging jets: p_T^{rel,j_1} and p_T^{rel,j_2} . This quantity is defined as follows:

- for each of the two tagging jets, we perform a longitudinal boost to a frame where the jet has zero rapidity.
- In this frame, we compute the quantity

$$p_T^{\text{rel},j} = \sum_{i \in j} \frac{|\vec{k}^i \times \vec{p}^j|}{|\vec{p}^j|}, \quad (3.8)$$

where k^i 's are the momenta of the particles that belong to the jet that, in this frame, has momentum p^j .

This quantity is thus the sum of the absolute values of the transverse momenta, taken with respect to the jet axis, of the particles inside the hardest jet, in the frame specified above.

As last comparison, we have studied the probability of finding a veto jet and we have compared this with the results of ref. [15]. For the central jet veto proposal, events are

discarded if any additional jet with a transverse momentum above a minimal value, $p_{T,\text{veto}}$, is found between the tagging jets. In ref. [15], the authors present a calculation of the dominant NLO correction to the production of a Higgs boson plus three jets, i.e. the LO of this correction coincides with the real contribution in this paper, since here we deal with NLO correction to Higgs boson production plus two jets.

In order to make a comparison with the results of ref. [15], we need to slightly adjust our cuts to the ones used in that paper. The cuts in eqs. (3.3) and (3.4) are replaced by the following

$$p_{Tj} > 20 \text{ GeV}, \quad |y_j| < 4.5, \quad (3.9)$$

and

$$p_T^{\text{tag}} > 30 \text{ GeV}, \quad |y_{j_1} - y_{j_2}| > 4, \quad y_{j_1} \cdot y_{j_2} < 0, \quad m_{jj} > 600 \text{ GeV}, \quad (3.10)$$

with jets reconstructed with resolution parameter $R = 0.8$. The Higgs boson decay products (generically called “leptons” in the following) are required to fall between the two tagging jets in rapidity and they should be well observable. While the exact criteria for the Higgs decay products will depend on the channel considered, such specific requirements here are substituted by generating isotropic Higgs boson decay into two massless “leptons” (which represent $\tau^+\tau^-$ or $\gamma\gamma$ final states) and requiring

$$p_{T\ell} \geq 20 \text{ GeV}, \quad |\eta_\ell| \leq 2.5, \quad \Delta R_{j\ell} \geq 0.6, \quad (3.11)$$

where $\Delta R_{j\ell}$ denotes the jet-lepton separation in the rapidity-azimuthal angle plane. In addition, the two “leptons” are required to fall between the two tagging jets in rapidity

$$\min(y_{j_1}, y_{j_2}) + 0.6 < \eta_{\ell_{1,2}} < \max(y_{j_1}, y_{j_2}) - 0.6. \quad (3.12)$$

Note that no reduction due to branching ratios for specific final states has been included in the calculation. In addition we set $\mu_F = \mu_R = 40 \text{ GeV}$, since this value minimizes the scale dependence of the NLO $Hjjj$ prediction and, at the same time, it provides optimal agreement between LO and NLO $Hjjj$ total cross sections, within the VBF cuts.

We are now in the position to make a comparison between our results and the ones in ref. [15] for the the probability, P_{veto} , of finding a veto jet

$$P_{\text{veto}} = \frac{1}{\sigma_2^{NLO}} \int_{p_{T,\text{veto}}}^{\infty} dp_T^{j,\text{veto}} \frac{d\sigma}{dp_T^{j,\text{veto}}}, \quad (3.13)$$

where $p_T^{j,\text{veto}}$ is the transverse momentum of the hardest veto jet, and $\sigma_2^{NLO} = 0.723 \text{ pb}$ is the total cross section (within VBF cuts) for $Hjjj$ production at NLO, computed with $\mu_F = \mu_R = m_H$. In fig. 10 we have plotted the LO and NLO $Hjjj$ curves of ref. [15], and the results we have obtained with POWHEG. We see that the results of POWHEG interfaced to HERWIG and PYTHIA are consistent with the LO band obtained with a change of the renormalization and factorization scale by a factor of two. In addition, notice that the distance between POWHEG+PYTHIA and POWHEG+HERWIG is comparable to the scale uncertainty of the leading order result.

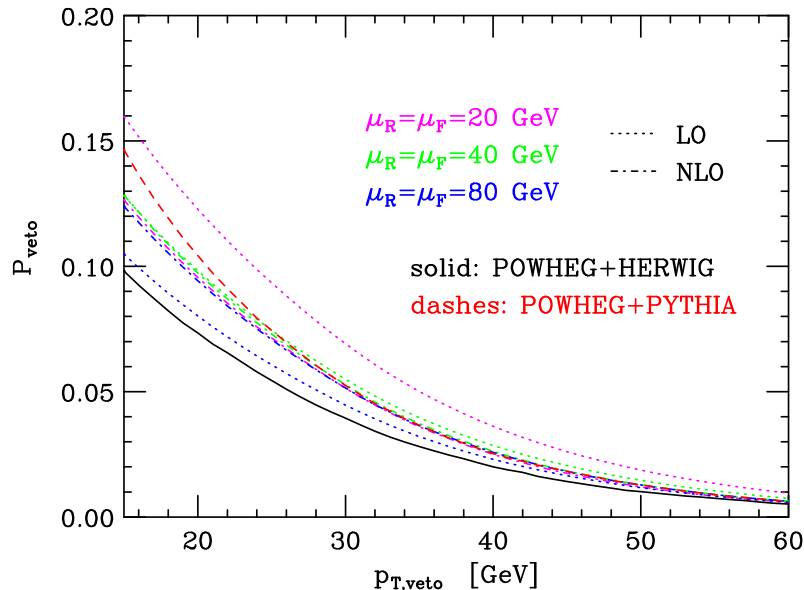


Figure 10: Probability of finding a veto jet defined as in eq. (3.13). The dotted curves depict the LO results and the dotdashed ones the NLO results for $Hjjj$ production, taken from ref. [15], for $\mu_F = \mu_R = 20$ GeV (magenta), $\mu_F = \mu_R = 40$ GeV (green) and $\mu_F = \mu_R = 80$ GeV (blue). The solid black and dashed red curves represent the results of POWHEG interfaced to HERWIG and PYTHIA.

4. Conclusions

In this paper we have described a complete implementation of Higgs boson production in vector-boson fusion at next-to-leading order in QCD, in the POWHEG framework. Together with $Z+1$ jet production [32], this is the first time that the NLO results for these processes are merged with a shower. The actual implementation is based on the POWHEG BOX package: this is an automated package designed to allow the construction of a POWHEG implementation for any given NLO calculation. New features with respect to previous implementations of POWHEG have been applied to deal with VBF Higgs boson production: the tagging of parton lines and the tuning of the real cross section in POWHEG.

We have shown and discussed several distributions after imposing typical VBF cuts (the two jets with highest transverse momentum must be well separated in rapidity, lie in opposite hemispheres and have a large invariant mass). These cuts strongly suppress many backgrounds to Higgs boson production via VBF, at the LHC.

We have showered the POWHEG outputs both with HERWIG and with PYTHIA and found good agreement between the two showers. Furthermore, we have found that overall our calculation confirms results obtained previously with parton-level Monte Carlo programs. We found some discrepancies between our POWHEG result showered with HERWIG and with PYTHIA in the multiplicity of final-state jets, for more than three jets.

The computer code for the POWHEG implementation presented in this paper will soon be available at the site <http://moby.mib.infn.it/~nason/POWHEG>, as part of the POWHEG BOX package.

References

- [1] CMS Collaboration, *CMS TDR, Report CMS/LHCC/2006-021, CMS TDR 8.2*.
- [2] ATLAS Collaboration, *ATLAS TDR, Report CERN/LHCC/99-15 (1999)*.
- [3] D. Zeppenfeld, R. Kinnunen, A. Nikitenko, and E. Richter-Was, *Measuring Higgs boson couplings at the LHC, Phys. Rev. D* **62** (2000) 013009, [[hep-ph/0002036](#)].
- [4] M. Dührssen *et al.*, *Extracting Higgs boson couplings from LHC data, Phys. Rev. D* **70** (2004) 113009, [[hep-ph/0406323](#)].
- [5] D. L. Rainwater, D. Zeppenfeld, and K. Hagiwara, *Searching for $H \rightarrow \tau\tau$ in weak boson fusion at the LHC, Phys. Rev. D* **59** (1999) 014037, [[hep-ph/9808468](#)].
- [6] T. Plehn, D. L. Rainwater, and D. Zeppenfeld, *A method for identifying $H \rightarrow \tau\tau \rightarrow e^\pm \mu^\mp p_T$ at the CERN LHC, Phys. Rev. D* **61** (2000) 093005, [[hep-ph/9911385](#)].
- [7] D. L. Rainwater and D. Zeppenfeld, *Observing $H \rightarrow W^{(*)}W^{(*)} \rightarrow e^\pm \mu^\mp p_T$ in weak boson fusion with dual forward jet tagging at the CERN LHC, Phys. Rev. D* **60** (1999) 113004, [[hep-ph/9906218](#)].
- [8] N. Kauer, T. Plehn, D. L. Rainwater, and D. Zeppenfeld, *$H \rightarrow WW$ as the discovery mode for a light Higgs boson, Phys. Lett. B* **503** (2001) 113–120, [[hep-ph/0012351](#)].
- [9] D. L. Rainwater and D. Zeppenfeld, *Searching for $H \rightarrow \gamma\gamma$ in weak boson fusion at the LHC, JHEP* **12** (1997) 005, [[hep-ph/9712271](#)].
- [10] T. Figy, C. Oleari, and D. Zeppenfeld, *Next-to-leading order jet distributions for Higgs boson production via weak-boson fusion, Phys. Rev. D* **68** (2003) 073005, [[hep-ph/0306109](#)].
- [11] V. Ravindran, J. Smith, and W. L. Van Neerven, *Next-to-leading order QCD corrections to differential distributions of Higgs boson production in hadron hadron collisions, Nucl. Phys. B* **634** (2002) 247–290, [[hep-ph/0201114](#)].
- [12] E. L. Berger and J. M. Campbell, *Higgs boson production in weak boson fusion at next-to-leading order, Phys. Rev. D* **70** (2004) 073011, [[hep-ph/0403194](#)].
- [13] K. Arnold *et al.*, *VBFNLO: A parton level Monte Carlo for processes with electroweak bosons, Comput. Phys. Commun.* **180** (2009) 1661–1670, [[0811.4559](#)].
- [14] <http://mcfm.fnal.gov>.
- [15] T. Figy, V. Hankele, and D. Zeppenfeld, *Next-to-leading order QCD corrections to Higgs plus three jet production in vector-boson fusion, JHEP* **02** (2008) 076, [[0710.5621](#)].
- [16] J. R. Andersen and J. M. Smillie, *QCD and electroweak interference in Higgs production by gauge boson fusion, Phys. Rev. D* **75** (2007) 037301, [[hep-ph/0611281](#)].
- [17] A. Bredenstein, K. Hagiwara, and B. Jäger, *Mixed QCD-electroweak contributions to Higgs-plus-dijet production at the LHC, Phys. Rev. D* **77** (2008) 073004, [[0801.4231](#)].
- [18] M. Ciccolini, A. Denner, and S. Dittmaier, *Electroweak and QCD corrections to Higgs production via vector-boson fusion at the LHC, Phys. Rev. D* **77** (2008) 013002, [[0710.4749](#)].
- [19] J. R. Andersen, T. Binoth, G. Heinrich, and J. M. Smillie, *Loop induced interference effects in Higgs Boson plus two jet production at the LHC, JHEP* **02** (2008) 057, [[0709.3513](#)].
- [20] P. Nason, *A new method for combining NLO QCD with shower Monte Carlo algorithms, JHEP* **11** (2004) 040, [[hep-ph/0409146](#)].

- [21] S. Frixione, P. Nason, and C. Oleari, *Matching NLO QCD computations with Parton Shower simulations: the POWHEG method*, *JHEP* **11** (2007) 070, [0709.2092].
- [22] P. Nason and G. Ridolfi, *A positive-weight next-to-leading-order Monte Carlo for Z pair hadroproduction*, *JHEP* **08** (2006) 077, [hep-ph/0606275].
- [23] S. Frixione, P. Nason, and G. Ridolfi, *A Positive-Weight Next-to-Leading-Order Monte Carlo for Heavy Flavour Hadroproduction*, *JHEP* **09** (2007) 126, [0707.3088].
- [24] O. Latunde-Dada, S. Gieseke, and B. Webber, *A positive-weight next-to-leading-order Monte Carlo for e^+e^- annihilation to hadrons*, *JHEP* **02** (2007) 051, [hep-ph/0612281].
- [25] O. Latunde-Dada, *Applying the POWHEG method to top pair production and decays at the ILC*, *Eur. Phys. J.* **C58** (2008) 543–554, [0806.4560].
- [26] S. Alioli, P. Nason, C. Oleari, and E. Re, *NLO vector-boson production matched with shower in POWHEG*, *JHEP* **07** (2008) 060, [0805.4802].
- [27] K. Hamilton, P. Richardson, and J. Tully, *A Positive-Weight Next-to-Leading Order Monte Carlo Simulation of Drell-Yan Vector Boson Production*, *JHEP* **10** (2008) 015, [0806.0290].
- [28] A. Papaefstathiou and O. Latunde-Dada, *NLO production of W' bosons at hadron colliders using the MC@NLO and POWHEG methods*, *JHEP* **07** (2009) 044, [0901.3685].
- [29] S. Alioli, P. Nason, C. Oleari, and E. Re, *NLO Higgs boson production via gluon fusion matched with shower in POWHEG*, *JHEP* **04** (2009) 002, [0812.0578].
- [30] K. Hamilton, P. Richardson, and J. Tully, *A Positive-Weight Next-to-Leading Order Monte Carlo Simulation for Higgs Boson Production*, *JHEP* **04** (2009) 116, [0903.4345].
- [31] S. Alioli, P. Nason, C. Oleari, and E. Re, *NLO single-top production matched with shower in POWHEG: s- and t-channel contributions*, *JHEP* **09** (2009) 111, [0907.4076].
- [32] S. Alioli, P. Nason, C. Oleari, and E. Re. To appear soon.
- [33] S. Frixione and B. R. Webber, *Matching NLO QCD computations and parton shower simulations*, *JHEP* **06** (2002) 029, [hep-ph/0204244].
- [34] G. Corcella *et al.*, *HERWIG 6: An event generator for hadron emission reactions with interfering gluons (including supersymmetric processes)*, *JHEP* **01** (2001) 010, [hep-ph/0011363].
- [35] G. Corcella *et al.*, *Herwig 6.5 release note*, hep-ph/0210213.
- [36] T. Sjostrand, S. Mrenna, and P. Skands, *Pythia 6.4 physics and manual*, *JHEP* **05** (2006) 026, [hep-ph/0603175].
- [37] S. Alioli, P. Nason, C. Oleari, and E. Re. To appear soon.
- [38] K. Hagiwara and D. Zeppenfeld, *Helicity Amplitudes for Heavy Lepton Production in e^+e^- Annihilation*, *Nucl. Phys.* **B274** (1986) 1.
- [39] K. Hagiwara and D. Zeppenfeld, *Amplitudes for Multiparton Processes Involving a Current at e^+e^- , $e^\pm p$, and Hadron Colliders*, *Nucl. Phys.* **B313** (1989) 560.
- [40] J. Pumplin *et al.*, *New generation of parton distributions with uncertainties from global QCD analysis*, *JHEP* **07** (2002) 012, [hep-ph/0201195].
- [41] V. Del Duca, W. Kilgore, C. Oleari, C. Schmidt, and D. Zeppenfeld, *$H + 2$ jets via gluon fusion*, *Phys. Rev. Lett.* **87** (2001) 122001, [hep-ph/0105129].

- [42] V. Del Duca, W. Kilgore, C. Oleari, C. Schmidt, and D. Zeppenfeld, *Gluon-fusion contributions to $H + 2$ jet production*, *Nucl. Phys.* **B616** (2001) 367–399, [[hep-ph/0108030](#)].
- [43] S. Catani, Y. L. Dokshitzer, M. H. Seymour, and B. R. Webber, *Longitudinally invariant k_T clustering algorithms for hadron-hadron collisions*, *Nucl. Phys.* **B406** (1993) 187–224.
- [44] M. Cacciari and G. P. Salam, *Dispelling the N^3 myth for the k_T jet-finder*, *Phys. Lett.* **B641** (2006) 57–61, [[hep-ph/0512210](#)].
- [45] T. Plehn, D. L. Rainwater, and D. Zeppenfeld, *Determining the structure of Higgs couplings at the LHC*, *Phys. Rev. Lett.* **88** (2002) 051801, [[hep-ph/0105325](#)].
- [46] V. Hankele, G. Klamke, and D. Zeppenfeld, *Higgs + 2 jets as a probe for CP properties*, [hep-ph/0605117](#).
- [47] G. Klamke and D. Zeppenfeld, *Higgs plus two jet production via gluon fusion as a signal at the CERN LHC*, *JHEP* **04** (2007) 052, [[hep-ph/0703202](#)].
- [48] V. Hankele, G. Klamke, D. Zeppenfeld, and T. Figy, *Anomalous Higgs boson couplings in vector boson fusion at the CERN LHC*, *Phys. Rev.* **D74** (2006) 095001, [[hep-ph/0609075](#)].
- [49] V. D. Barger, R. J. N. Phillips, and D. Zeppenfeld, *Mini-jet veto: A Tool for the heavy Higgs search at the LHC*, *Phys. Lett.* **B346** (1995) 106–114, [[hep-ph/9412276](#)].
- [50] D. L. Rainwater, R. Szalapski, and D. Zeppenfeld, *Probing color singlet exchange in $Z + two$ jet events at the CERN LHC*, *Phys. Rev.* **D54** (1996) 6680–6689, [[hep-ph/9605444](#)].
- [51] V. Del Duca, A. Frizzo, and F. Maltoni, *Higgs boson production in association with three jets*, *JHEP* **05** (2004) 064, [[hep-ph/0404013](#)].
- [52] V. Del Duca *et al.*, *Monte Carlo studies of the jet activity in Higgs + 2 jet events*, *JHEP* **10** (2006) 016, [[hep-ph/0608158](#)].
- [53] J. R. Andersen, V. Del Duca, and C. D. White, *Higgs Boson Production in Association with Multiple Hard Jets*, *JHEP* **02** (2009) 015, [[0808.3696](#)].